Synchrotron-based x-ray diffraction analysis of energetic ion-induced strain in GaAs and 4H-SiC

Anusmita Chakravorty, Alexandre Boulle, Aurélien Debelle, Gouranga Manna, Pinku Saha, D. Kanjilal, Debdulal Kabiraj

Synchrotron-based X-ray diffraction analysis of energetic ion-induced strain in GaAs and 4H-SiC

Anusmita Chakravorty,[1, 2, a)] Alexandre Boulle,[3] Aurélien Debelle,[4] Gouranga Manna,[5, 6] Pinku Saha,[5, 7] D. Kanjilal,[1] and Debdulal Kabiraj[1, b)]

[1)] *Inter-University Accelerator Centre, Aruna Asaf Ali Marg, New Delhi-110067, India*

[2)] *The Pennsylvania State University, University Park, PA, 16802, USA*

[3)] *Institut de Recherche sur les Céramiques (IRCER), CNRS UMR 7315, 12 rue Atlantis, Cedex, Limoges 87068, France*

[4)] *IJCLab, Université Paris-Saclay, CNRS/IN2P3, Institut de Physique des 2 Infinis Irène Joliot-Curie, Orsay 91405, France*

[5)] *Chemistry and Physics of Materials Unit, Jawaharlal Nehru Centre for Advanced Scientific Research, Rachenahalli Lake Rd, Jakkur, Bengaluru, Karnataka 560064, India*

[6)] *ESRF - The European Synchrotron, 38043 Grenoble, France*

[7)] *Department of Earth Sciences, ETH Zürich, Zürich 8092, Switzerland*

(Dated: 3 May 2024)

Strain engineering using ion beams is a current topic of research interest in semiconductor materials. Synchrotron-based–high-resolution X-ray diffraction has been utilized for strain-depth analysis in GaAs irradiated with 300 keV Ar, and 4H-SiC and GaAs irradiated with 100 MeV Ag ions. The direct displacement-related defect formation, anticipated from the elastic energy loss of Ar ions, can well explain the irradiation-induced strain depth profiles. The maximum strain in GaAs is evaluated to be 0.88% after Ar irradiation. The unique energy loss depth profile of 100 MeV Ag (swift heavy ions; SHIs), and resistance of pristine 4H-SiC and GaAs to form amorphous/highly disordered ion tracks by ionization energy loss of monatomic ions, allow us to examine strain buildup due to the concentrated displacement damage by the elastic energy loss near the end of ion range (~ 12 μm). Interestingly, for the case of SHIs, the strain-depth evolution requires consideration of recovery by ionization energy loss component in addition to the elastic displacement damage. For GaAs, strain builds up throughout the ion range, and the maximum strain increases and then saturates at 0.37% above an ion fluence of 3×10^{13} Ag/cm^2. Whereas, for 4H-SiC, the maximum strain reaches 4.6% and then starts to recover for fluences above 1×10^{13} Ag/cm^2. Finally, the contribution of irradiation defects and the purely mechanical contribution to the total strain have been considered to understand the response of different compounds to ion irradiation.

I. INTRODUCTION

Advances in the practical application of ion irradiation require extensive research to better understand and utilize ion beam-induced effects in materials. Over the past decades, continuous research using energetic ion beams has been carried out in various materials[1]. Ion beam modification has evolved as a popular method for improving or designing materials for advanced applications, ranging from ion doping to testing of materials for nuclear and space environments. In the semiconductor industry, ion implantation has established itself as the most suitable tool to precisely control the dose and depth of the implanted dopants[2]. Another ability of ion irradiation that has attracted research is to generate controlled defects in materials by elastic collisions leading to atomic displacements[1]. The energy loss responsible for such displacement collisions is termed the nuclear stopping power which dominates for low energy (keVs to a few MeVs) irradiation. High-energy heavy ions (energy $\geq$ 1 MeV/amu) are often called 'Swift heavy ions (SHIs)', and the energy loss mechanism for SHIs is dominated by an inelastic collision between the projectile ion and the electrons of the target. The energy loss responsible for such ionization or electronic excitations is called the electronic stopping power. Thus, for thin film doping and other physico-chemical surface modifications, low energy ions are utilized whereas, SHIs find applications in structural modifications at a sub-surface region or in replication of extreme conditions like that of fission fragments emitted in nuclear reactors, defense technologies, and cosmic radiation environment. SHI irradiation has also emerged as a suitable method for producing uniform and low defect concentrations within several micrometers from the surface in certain materials like SiC and GaAs where ionization energy loss by monatomic ions does not result in amorphous or highly disordered ion tracks[3,4]. Additionally, SHIs have also shown the potential to recover these pre-damaged crystalline materials, allowing the annealing of undesirable defects[5,6].

The traditional silicon-based devices typically do not achieve high enough breakdown voltages due to the low critical field strength. Thus, the technological requirement for high-performance devices demands a replacement of silicon-based electronics with higher bandgap

[a)] Electronic mail: anusmitachakravorty@gmail.com

[b)] Electronic mail: kabiraj@iuac.res.in

materials like SiC and GaN[7]. Devices made of GaN or SiC have a greater critical field strength but suffer from low electron carrier mobilities, resulting in relatively significant resistive losses and a high cost since good quality large-area substrates are either unavailable or excessively expensive. Recent advancements demonstrated that using GaAs technology, comparable outcomes to SiC and GaN may be obtained at substantially lower component prices[8–10]. GaAs, with considerably higher electron mobilities, has been demonstrated to offer lower series resistance and consequently lower power consumptions in the "on" state than Si, GaN, or SiC. Over the years, SiC has emerged as a suitable candidate for high-power devices, operating at voltages above 800 V whereas, GaAs has attracted attention for high-frequency applications, owing to its superior mobility. Significant experimental efforts have been made recently to study ion irradiation-induced–defect-related strain in 4H-SiC and GaAs for controlled modifications[11–13]. One of the approaches that have gained importance for controlled tuning of the structural strain in semiconductors is ion irradiation/implantation. This in turn allows post-growth modifications of the optical and transport characteristics of bulk and epitaxial semiconductors, exploration of which is beyond the scope of this work.

Despite decades of research, fundamental problems involving ion-solid interactions remain unresolved, one of which is the lattice strain growth kinetics in ion-irradiated materials. The present study explores two technologically important materials that differ significantly in terms of crystalline structure. The study compares the radiation-induced strain (i.e. the relative change in lattice parameter) in GaAs and 4H-SiC single crystals after irradiation with low-energy 300 keV Ar ions and high-energy 100 MeV Ag. For the objective of analyzing strain depth profiles, a very sensitive Synchrotron-based high-resolution (HR-XRD) method has been adopted. Due to the monochromatic high flux and higher collimation, this experimental probing approach is more efficient than a standard lab-based XRD, enabling the detection of otherwise undetectable signals[14]. Further, to identify the irradiation-induced structural and chemical disorders that are responsible for the observed strain in the crystals, Channeling-Rutherford backscattering (C-RBS) and Raman scattering spectroscopy analysis on the same samples have been taken into consideration.

II. EXPERIMENT

For experiments, the commercially available single-crystal wafers of GaAs and 4H-SiC were cut in sizes of 1×1 cm^2. Before irradiations, TRIM full-cascade simulations[15,16] were performed to predict the experimental parameters such as the ion beam energy, range, and fluence (ions/cm^2). The room temperature irradiations were performed with low energy 300 keV ions at LEIBF, Inter-University Accelerator Centre in New Delhi, India. To compare the induced strain, the same levels of damage were introduced using the TRIM estimated maximum displacements per atom (dpa; 1 dpa = denotes reaching the state of complete amorphization) values. In TRIM simulations: (i) the density of 4H-SiC was taken as 3.21 g/cm^3, with threshold displacement energies of 20 and 35 eV for the C and Si sublattices[17], respectively, and (ii) the density of GaAs was taken as 5.32 g/cm^3, with threshold displacement energies of 10 eV for both As and Ga[18]. The fluences corresponding to maximum dpa values of 0.1, 0.7, and 1 dpa were chosen for this experimental work. For high-energy irradiations involving 100 MeV Ag ions, the 15-UD Pelletron accelerator facility in IUAC was utilized. These irradiations were performed at liquid nitrogen temperature (∼80 K) to prevent any influence of external heating. Both materials were subjected to the same Ag fluences ranging from 1×10^{12} to 6×10^{13} Ag/cm^2. During the experiment, ion currents were maintained at 100 particle nanoampere (pnA; 1pnA= 6.25×10^9 ions/s) for low energy Ar and 1 pnA for high energy Ag to avoid excessive heating of the targets. The beam was raster scanned on the samples.

The HR-XRD measurements were performed using the synchrotron X-rays of wavelength 1.2384 $\mathring{A}$ at 18B KEK beamline facility, Photon Factory, Japan. For a proper alignment, multiple loop scans (symmetrical rocking scans) were performed to get the maximum intensity in the detector. Finally, when the alignment was completed for the desired Bragg reflection, the high-resolution diffraction data was collected by using coupled 2θ-θ scans with a θ resolution of 0.001°. The obtained data were simulated using the RaDMaX program to extract information about the elastic strain depth profiles[19,20]. C-RBS spectra were recorded using 2 MeV He^+ ions at the Pelletron Accelerator RBS-AMS Systems (PARAS) facility at IUAC, New Delhi, India.

III. RESULTS AND ANALYSIS

A. 300 keV Ar irradiations at room temperature

Based on TRIM simulations[15,16] and previously reported[21–24] C-RBS results for 300 keV ions in 4H-SiC and GaAs, the ion range is about 350 nm with the damage peak at around 175 nm. For both of these materials, the damage builds up in two steps and the onset of the second step is observed at 0.3 dpa[21]. The corresponding irradiation-induced elastic strain has been evaluated by monitoring the XRD signals near the 004 and 400 Bragg reflections for 4H-SiC and GaAs, respectively. These reflections provide the best balance between scattered intensity and resolution.

Fig. 1(a) presents the HR-XRD profiles of pristine and Ar-irradiated GaAs crystals. Since the damaged depth for 300 keV Ar ion irradiation in GaAs is substantially less than the X-ray penetration depth, contribution from

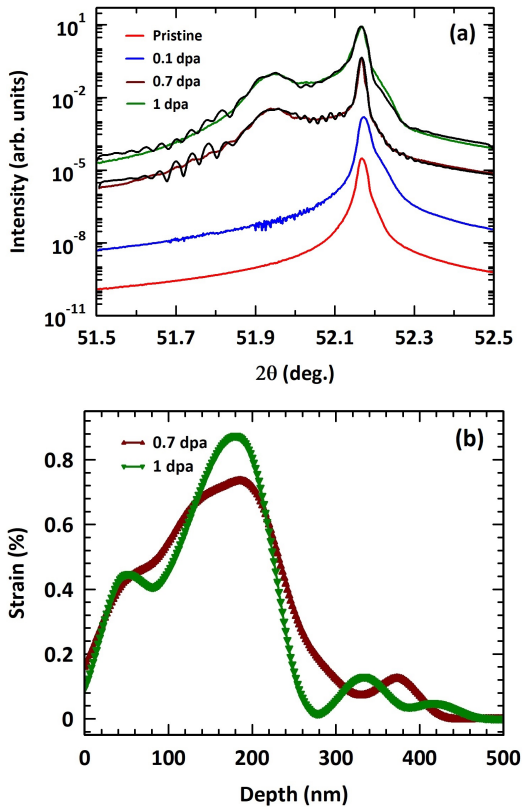

FIG. 1. (a) Evolution of the 400 peak in HR-XRD profiles of GaAs irradiated with fluences of 2.3×10^{13} ions/cm^2 (0.1 dpa), 1.6×10^{14} ions/cm^2 (0.7 dpa) and 2.3×10^{14} ions/cm^2 (1 dpa) using 300 keV Ar ions. The black lines are simulated curves and the colored lines represent the experimental data. (b) The corresponding strain profiles obtained after simulating the HR-XRD data.

the underlying substrate cannot be eliminated. But on the other hand, it's highly useful to evaluate the strain, as it's a reference. The 2θ position of 400 Bragg peak for the pristine crystal is detected at an angle of 52.17°. The obtained HR-XRD profile for the 0.1 dpa crystal exhibits no detectable strain-related signal in the diffraction pattern probably due to the generation of very low defect concentrations at such low doses. This observation is further supported by the corresponding C-RBS and Raman profiles (presented in Refs.[21,22]), showing almost negligible structural and chemical lattice disordering for 0.1 dpa GaAs. However, an asymmetric broadening of the Bragg peak, resulting from an additional shoulder peak at a slightly higher angle of 2θ can be observed in Fig. 1(a), suggesting that irradiation-induced defects have caused a structural change by locally shortening the lattice spacings. Since this feature is already present in the pristine crystal, it is most likely due to the intrinsic defects that are magnified upon irradiation. This points to the presence of some vacancy-like isolated point defects[25,26]. For 0.7 dpa crystal, in addition to the Bragg peak, a broad feature with some oscillations can be noticed in the HR-XRD pattern in the lower 2θ angles, indicating the presence of a dilatation gradient in the interplanar spacings of the crystal lattice perpendicular to the surface. The dominance of interstitial-like defects[26] can be held responsible for causing some lattice expansion which is prominently reflected in the XRD data for 0.7 dpa GaAs. The oscillations observed on the XRD scan arise from interferences between scattered beams emerging from the damaged part of the crystal, and the fringe spacing is related to the width of the strained region for a given strain level. A similar profile can be seen for the 1 dpa crystal but with no detectable oscillations in the diffraction pattern, most likely because of random strain variations (i.e. microstrain) which broaden the signal and hence blur out fine details in the XRD curves. Recently, various studies showed that as the damage in GaAs increases from 0.7 dpa to 1 dpa, the crystal moves from a highly disordered state to complete amorphization[3,4,21,22].

The strain profiles evaluated after simulation of the XRD curves with the RaDMaX program[19,20] are presented in Fig. 1(b). The strain is presumably too low to be detected at 0.1 dpa because no such significant strain-related signals like oscillations or well-defined distinct peaks from the damaged region could be recorded. The strain profiles were determined with a reasonably good agreement of the simulated profiles for the HR-XRD data of 0.7 and 1 dpa crystals. The unusual oscillations in the strain profiles beyond 300 nm are because the (dynamical) theory on which RaDMaX is based does not account for microstrains that produce the additional broadening. Another possible reason is that the XRD data does not have sufficient information as the interference fringes are barely visible at 0.7 dpa and absent at 1 dpa. The retrieved strain profiles indicate that the strain for 0.7 dpa crystal peaks at a value of 0.72% at around 175 nm which increases to 0.88% for 1 dpa crystal. As shown in supplementary Fig. S1, in the case of 4H-SiC, as the damage increased from 0.1 to 0.7 dpa, the maximum strain increased from 1% to 12% but the position of the strain maximum remained fixed. When the damage increased from 0.7 to 1 dpa, the lattice strain achieved a high maximum saturation value of 12% with essentially identical strain profiles. This suggested that the strain saturated after the incorporation of extended amorphous layers in the damaged region in 4H-SiC. However, for GaAs, the obtained strain does not show any saturation in contrast to the observations made for Ar irradiated 4H-SiC[14]. This is expected because it has been recently reported that the strain saturation for GaAs starts at a dpa value above 1[13]. For the same dpa values, the observed strain maximum in 4H-SiC is much higher than in GaAs. It can be concluded that as soon as the amorphous extended region builds up in 4H-SiC, the strain saturates at a value of about 12% whereas in GaAs it only reaches 0.88%.

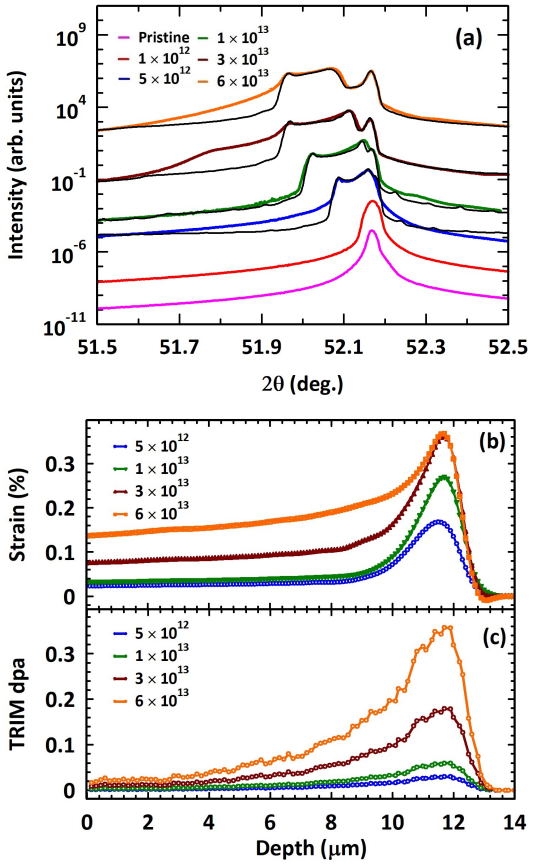

FIG. 2. (a) Evolution of the 400 peak in HR-XRD profiles of GaAs irradiated with 100 MeV Ag at ∼77K using various indicated fluences. The black lines are simulated curves and the colored lines represent the experimental data. (b) The corresponding strain profiles were obtained from the simulation of HR-XRD data. (c) The variation of TRIM[15,16] dpa with depth.

B. 100 MeV Ag irradiations at ∼80K

In Fig. 2(a), HR-XRD profiles obtained after Ag irradiation of GaAs crystals are shown. As the Ag fluence increases, initially the Bragg peak broadens and another broad shoulder band appears in the lower 2θ region, indicating strain buildup due to lattice expansion. The simulation of HR-XRD profiles was not straightforward due to the complex behavior of the data. The presence of an additional signal at lower angles in Fig. 2(a), posed a major challenge. Similar features have been previously observed after irradiation of GaAs with 100 MeV Ag[27]. In the present case, considering that this signal is two orders of magnitude weaker in intensity and much broader than the central part of the signal, we hypothesize that it emanates from highly strained clusters of nanometric size. The lack of any information regarding the spatial distribution of such clusters did not allow us to integrate this feature into the simulations. Therefore, we chose to neglect this part of the signal and focus only on the central part, from which it was possible to extract a meaningful evolution of the strain profiles. Although imperfect, this procedure nonetheless allowed us to obtain strain profiles that are in good agreement with TRIM simulations. Fig. 2(b) shows that the strain increases above irradiation fluence of 5×10^{12} Ag/cm^2 and then begins to saturate above 3×10^{13} Ag/cm^2. For the crystal irradiated with the lowest fluence of 1×10^{12} Ag/cm^2, the strain is probably too low to be detected by HR-XRD. The obtained strain profiles reveal that the lattice is significantly strained, starting from the surface to a depth of about 13 μm. In Fig. 2(c), the TRIM simulated damage profiles predict that the dpa value at the near-surface region is much less than 0.1 dpa, for all the samples. Also, the C-RBS results[22] support the absence of detectable structural disorder in the near-surface (upto ∼1μm) region of the irradiated samples. Interestingly, for the samples irradiated with fluences of 5×10^{12} Ag/cm^2 and 1×10^{13} Ag/cm^2, the dpa values near the end ion's range are still less than 0.1 dpa yet considerable strain develops as shown in Fig. 2(b). The strain developed, on the other hand, is less than the experimental detection limit for a comparable dpa value of 0.1 introduced by 300 keV Ar ions Fig 1(a). Here, it may be argued that heavier Ag ions cause denser collision cascades, which result in more complex defects for the same TRIM simulated dpa and reduce the probability of lattice recovery via defect recombinations.

The HR-XRD profiles obtained after Ag irradiation of 4H-SiC crystals are shown in Fig. 3(a). With increasing Ag fluence, additional diffraction signals appear on the low-angle side of the pristine 4H-SiC Bragg peak, suggesting an increase in interplanar spacing in the direction perpendicular to the surface. The broad extension of this signal towards lower angles suggests a very high level of strain. Interestingly, as the fluence is increased above 1×10^{13} Ag/cm^2, the strain-related signals begin to move towards the direction of the primary Bragg peak, which is direct evidence of strain relaxation in the irradiated region. At fluences of 3×10^{13} and 6×10^{13} Ag/cm^2, the broad peak progressively transforms into a well-defined peak close to the Bragg peak, indicating significant lattice recovery. This evolution is confirmed by the evolution of the strain profile in Fig. 3(b). In other words, some lattice sites are recovering and approaching the original lattice structure of the crystal. The corresponding strain profiles, presented in Fig. 3(b), show that the strain maximum is reached at a depth of ∼10 μm after Ag irradiation. From Figs. 3(b) and 3(c), it is evident that maximum strain is localized near the defective end of the ion's range, for 100 MeV Ag in 4H-SiC. However, damage buildup at such deeper depths (∼10 μm) cannot be studied by other experimental techniques like Raman and C-RBS. Moreover, a direct comparison is not straightforward, as different techniques have different sensitivities to the damage; for instance, amorphous pockets induce a significant increase in the backscattering yield and a typical signal in Raman, but almost nothing

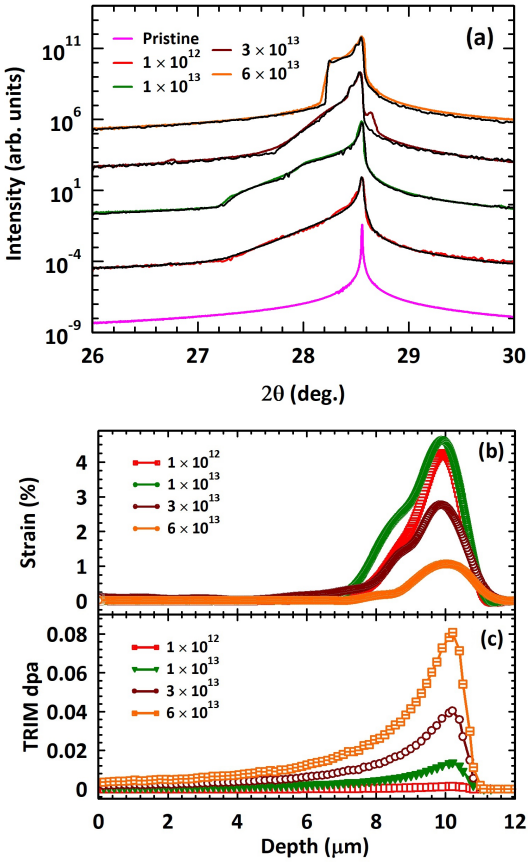

FIG. 3. (a) Evolution of the 004 peak in HR-XRD profiles of 4H-SiC irradiated with 100 MeV Ag at ∼77K using various indicated fluences. The black lines are simulated curves and the colored lines represent the experimental data. (b) The corresponding strain profiles were obtained from the simulation of HR-XRD data. (c) The variation of TRIM[15,16] dpa with depth.

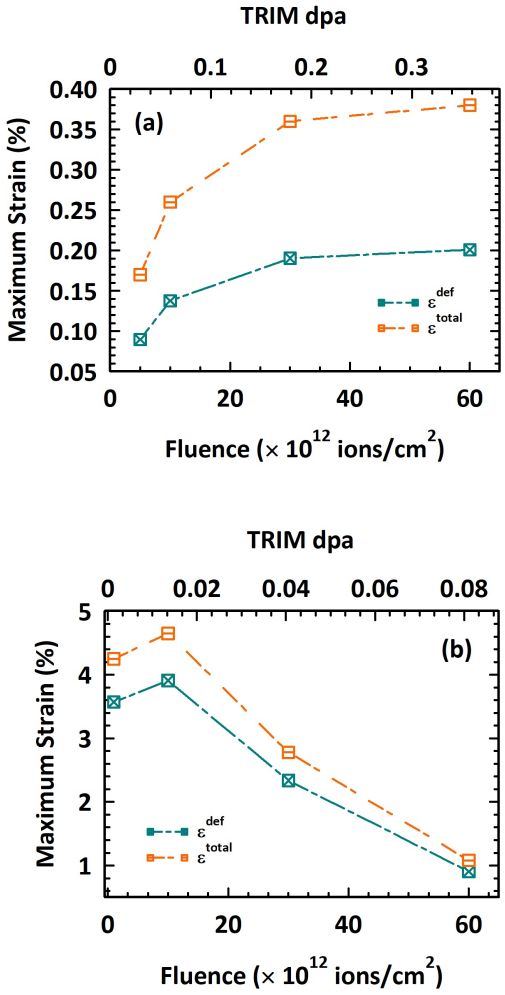

FIG. 4. Variation of maximum total strain (ϵ^{total}) and the strain due to defects (ϵ^{def}) in 100 MeV Ag irradiated (a) GaAs and (b) 4H-SiC with irradiation fluence. The TRIM[15,16] dpa values are indicated on top x-axis.

in XRD.

Finally, maximum total strain (ϵ^{total}) versus fluence is plotted for both GaAs and 4H-SiC. For GaAs, the strain maximum (shown in Fig. 4(a)), observed at a depth of 11.5 μm, varies from 0.17% to 0.37%. Within the range of experimental fluences used in this work, the strain appears to enter saturation at higher irradiation fluences (above 3 × 10^{12} Ag/cm^2). For 4H-SiC (shown in Fig.4(b)), initially, the maximum strain increases to 4.6 % with fluence; however, the strain goes on decreasing for fluences above 1 × 10^{13} Ag/cm^2.

IV. DISCUSSION

A. Strain saturation/recovery due to SHI - 'Ultrafast Thermal Spike'

The inelastic energy loss, also referred to as electronic stopping power (S_e), is the principal energy dissipation process that occurs during SHI irradiation; however, near the end of the ion range, the nuclear-stopping power (S_n) that causes direct elastic displacement damage, becomes significantly dominating. Thus, evaluation of the surface, as well as the sub-surface strain for SHI irradiation, sometimes requires consideration of both the energy loss processes. The synergistic effects due to the coupling of displacement cascades and ionization can lead to incascade-annealing *via* ionization-activated–thermally-assisted–defect-annealing (IATADA) process which can lead to dynamic recovery beyond certain S_e threshold values[3,28,29]. The TRIM simulated energy loss profiles for 100 MeV in 4H-SiC and GaAs are shown in Figs. 5(a) and 5(b). The value of S_e at the position of maximum strain is 2.25 keV/nm for 4H-SiC and 1.57 keV/nm for GaAs. As determined by Xue et. al.[29] and Zang et. al.[28], the threshold for IATADA in SiC is S_e ∼1.0 keV/nm. The IATADA can be considered as the mechanism to justify the observed strain reduction for higher

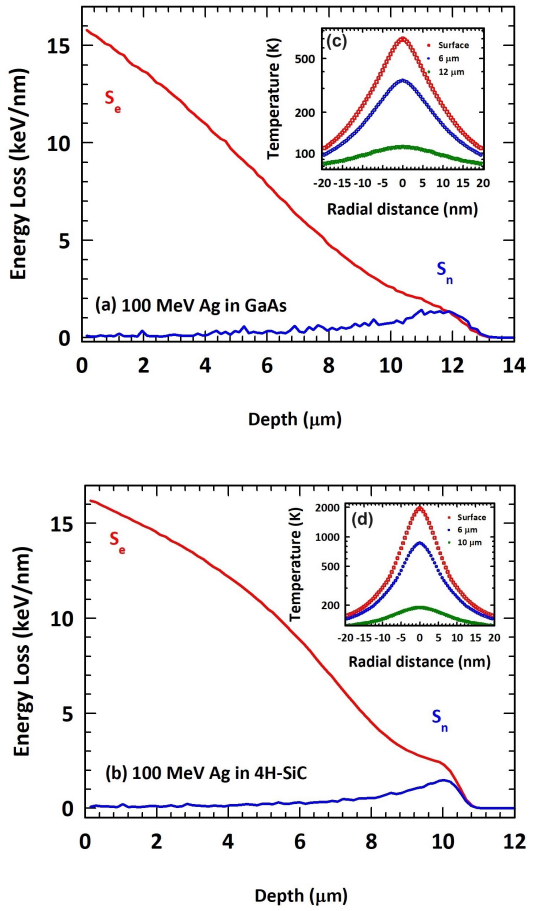

FIG. 5. TRIM simulated energy loss profiles for 100 MeV Ag in (a) GaAs and (b) 4H-SiC. Inset presents the thermal spike model outputs at 0.2 ps after ion impact in (c) GaAs and (b) 4H-SiC.

fluences in 4H-SiC. To our knowledge, for the case of GaAs, extensive research has not been conducted focused on studying the IATADA mechanism. However, in a recent work using dual-beam irradiation of GaAs, there was a defect annihilation effect by S_e[4]. Also, our work on SHI irradiation of pre-damaged GaAs showed a significant ionization stimulated damage recovery[22]. Since, in the present study, there is no strain recovery observed for GaAs, it can be stated that the S_e value of 1.57 keV/nm (at the depth of max. strain) is not large enough to result in IATADA. The present work demonstrates that 100 MeV Ag ions are efficient in preventing higher strain development in GaAs, and strain recovery in 4H-SiC beyond a certain fluence.

At considerably higher ion energies (MeVs to GeVs) where S_e dominates, an inelastic thermal spike model (TSM) can represent the connection between S_e mechanisms and atomic processes[30]. The S_e of the incoming ion causes significant electronic excitations and electron-electron scattering along its path. In the TSM, it is assumed that S_e is deposited instantaneously in a very small region, producing a localized increase in the electronic temperature which is then transferred by electron-phonon interactions from the electronic subsystem to the atomic subsystem of the target atoms. This energy spreads and dissipates according to the laws of classical heat conduction in a continuum, leading to a localized thermal spike. A thermal spike is a high-temperature region, along the ion trajectory, inside the material. The TSM gives a detailed description of the coupled electronic and atomic subsystems by a set of two heat diffusion equations. The coupled heat diffusion equations that describe the spatial and temporal evolution of the atomic temperature (T_a) and electronic temperature (T_e) are given as:

$$C_e\frac{\partial T_e}{\partial t} = \frac{1}{r}\frac{\partial}{\partial r}\left[rK_e\frac{\partial T_e}{\partial r}\right] - g(T_e - T_a) + A(\vec{r},t) \quad (1)$$

$$C_a\frac{\partial T_a}{\partial t} = \frac{1}{r}\frac{\partial}{\partial r}\left[rK_a\frac{\partial T_a}{\partial r}\right] + g(T_e - T_a) \quad (2)$$

where, T_e : electronic temperature (K)
T_a : atomic temperature (K)
C_e : heat capacity of the electronic system (J g^{-1} K^{-1})
C_a : heat capacity of the atomic system (J g^{-1} K^{-1})
K_e : electronic thermal conductivity (W cm^{-3} K^{-1})
K_e : lattice thermal conductivity (W cm^{-3} K^{-1})
A($\vec{r}$,t) : this term describes the energy deposition from the incident SHI to the electronic subsystem (W cm^{-3})
g: electron-phonon coupling parameter which controls the flux of heat or energy from the electrons to the phonons per unit time and volume (W cm^{-3} K^{-1})

Amorphization or drastic lattice disordering of 4H-SiC and GaAs has not been observed using monatomic SHI irradiation. However, in the case of existing pre-damage, these materials have been experimentally observed to show recovery effects[22–24]. This suggests that the IATADA process is capable of annealing some of the lattice defects created by nuclear-stopping power (S_n) of a single SHI in these materials. The local thermal spikes caused by SHI encourage lattice recovery, which leads to a competition between annealing by S_e and defect formation by S_n. Often, damage annealing is more pronounced than damage creation during SHI irradiation. This might result in saturation of the disorder or allow the disorder to be reduced. The TSM equations are solved to generate the local heating profiles from S_e at various depths. The thermodynamical parameters for solving the TSM equations for crystalline GaAs and 4H-SiC are taken from Refs.[22,23]. Thermal spike-generated outputs, 0.2 ps after ion impact, showing maximum radial temperature profiles at various depths, are presented as inset to Figs. 5(a) and 5(b). For both GaAs (1513 K) and 4H-SiC (3500 K) the temperature spikes do not exceed the melting temperature at the depth of maximum strain. Thus, the possibility of recovery at the crystalline-disorder interface via melting and rapid re-solidification, which is typically given as the explanation for thermal

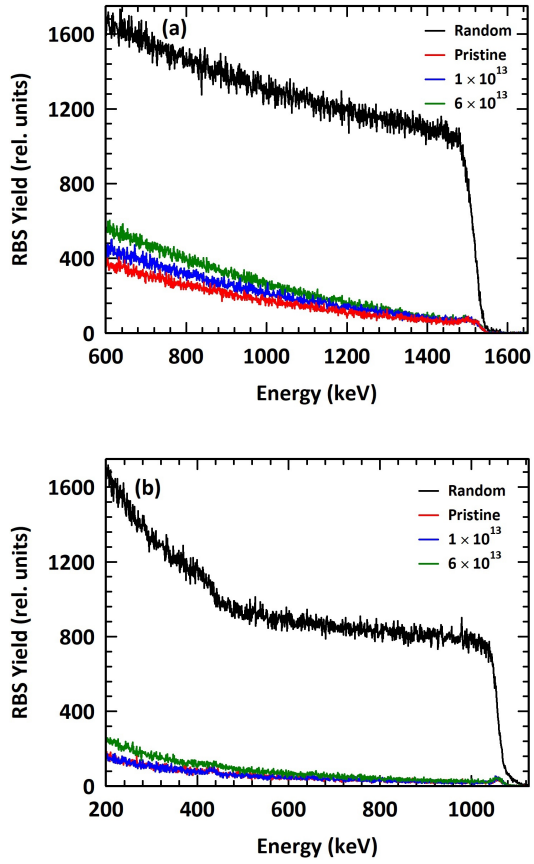

FIG. 6. Rutherford backscattering spectra recorded in a channeled condition on (a) GaAs and (b) 4H-SiC irradiated with 100 MeV Ag ions. The units of indicated ion fluences are in ions/cm^2.

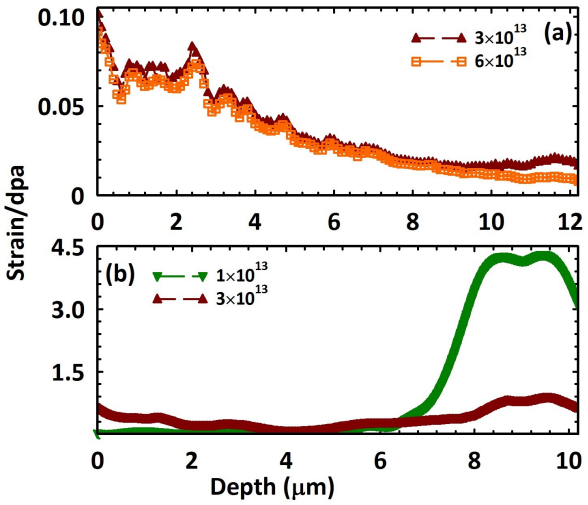

FIG. 7. Strain per dpa (dpa is the estimated damage fraction using TRIM simulations) (a) GaAs and (b) 4H-SiC irradiated with 100 MeV Ag ions. The units of indicated ion fluences are in ions/cm^2.

spike-induced recovery, is ruled out. However, defects can undergo thermal annealing when there is enough energy to cause migration and permit different recombination processes between pairs of defects[31]. The observed strain saturation for GaAs and strain recovery for 4H-SiC suggest that there is some defect recombination mechanism in action. The obtained thermal spikes are possibly allowing some solid-state defect migration for achieving lattice recovery. This explains the underlying mechanism behind IATADA. While strain recovery can be observed for 4H-SiC throughout the entire ion range, surface strain for GaAs does not saturate; rather, it grows almost linearly. This indicates that the thermal spike does not significantly impact the surface region even though it has a higher temperature peak.

B. Understanding surface strain

SHI irradiation uses its unique energy loss to induce deeper elastic displacement damage without adversely damaging the near-surface region. The S_n *vs.* depth in Figs. 5(a) and 5(b), and the corresponding dpa *vs.* depth profiles in Figs. 2(c) and 3(c) indicate that most of the lattice damage is confined near the end of the ion range and the near-surface dpa levels are negligibly small to account for any considerable lattice strain. To monitor the surface damage, C-RBS spectra were obtained on GaAs and 4H-SiC after irradiation with 100 MeV Ag as shown in Figs. 6(a) and 6(b). It can be concluded that the C-RBS spectra obtained following Ag ion irradiation at different fluences effectively overlap for higher energy channels, indicating that SHI did not cause any appreciable surface damage. The slight rise in the channeling yield, especially at low energy channels can be due to the generation of radiation defects at deeper depths. To further understand this, we derived strain per dpa profiles for samples after Ag irradiation of GaAs and 4H-SiC (presented in Figs. 7(a) and 7(b)). Strain per dpa means that the strain level is normalized to the dpa level along the damaged thickness. For 4H-SiC, the strain per dpa evolves according to the S_n *vs.* depth profiles, implying that the higher the dpa, the higher the elastic strain. However, for GaAs, the strain per dpa does not follow the same trend. As the corresponding curve is similar to the dpa profile for SiC and not for GaAs, one can infer that the strain is related to S_n essentially in SiC and that the elastic response to defect creation in GaAs is much more subtle, depending more widely on both Sn and Se. It can also be suggested that GaAs is less resistant to S_e (with regard to defect creation). The response of both the materials in terms of strain is different for several reasons. First, the difference in elastic properties but this is expected to play only an effect on the magnitude. Second, the type of defects created upon S_n irradiation. If there is a difference between the defects created in the two materials, then the associated strain will be different as well. Third, the recovery by S_e depends on the

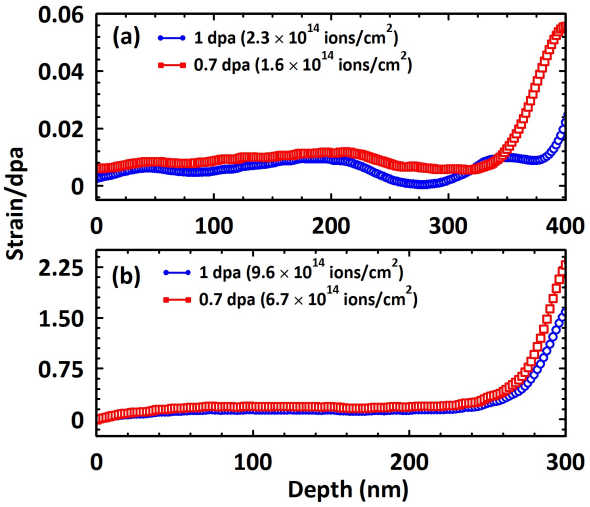

FIG. 8. Strain per dpa (dpa is the estimated damage fraction using TRIM simulations) in (a) GaAs and (b) 4H-SiC irradiated with indicated fluences using 300 keV Ar ions.

local damage state, and this latter is different for the two materials at the same dpa.

To better understand strain evolution owing to displacement damage in the S_n regime by low energy ions, the strain per dpa profiles produced by 300 keV Ar ions have been also analyzed and displayed in Figs. 8(a) and 8(b). The TRIM dpa *vs*. depth profiles are presented in supplementary Fig. S2. For both the materials under study, the strain per dpa plots is almost flat up to ~250 nm, demonstrating that strain increases almost linearly as damage increases. However, near the end of the ion range, right before the strain decreases to zero (i.e. relaxed lattice values), the strain increases sharply. The implantation of the incident ions in the target lattice and the contribution of the substrate reaction, as explained in the next section, may be the causes of this strain buildup.

C. Defect strain and rigid substrate contribution

It is worth noting that only a shallow layer (between a few tens of nanometers and a few tens of micrometers) at the specimen surface is affected by the irradiation process when extremely energetic ions (usually with a few MeV/nucleon) are utilized. As a result, it makes sense to think of the material as a thin (irradiated) layer on a substrate, with the undamaged portion of the crystal serving as the substrate. In this instance, it has been proven that a two-step model may adequately characterize the mechanical response of the sample[32,33]. The mechanical properties of the thick substrate beneath the irradiated layer prevent any lateral macroscopic dimensional change and the thin irradiated layer is subjected to an in-plane biaxial compressive stress. This completely cancels out the in-plane components of the strain $\epsilon^{def}_{(hkl)}$, which is caused by irradiation defects. Due to the rigid substrate contribution (RSC) caused by the Poisson effect, the growth of stress causes an extra tensile-strain contribution $\epsilon^{RSC}_{(hkl)}$ in the direction normal to the surface (out-of-plane strain). This contribution depends upon the elastic constants of the material and is proportional to $\epsilon^{def}_{(hkl)}$. As a result, the RSC can change depending on the (i) elastic constants of two distinct materials and (ii) crystallographic orientation of a crystal that is elastically anisotropic. Therefore, as the total strain is what is experimentally measured, it is necessary to take into account this purely mechanical contribution to compare the reaction of various materials to irradiation. Rao and Houska developed a model in the early 1990s to separate the two strain contributions in ion-irradiated materials[33]. Debelle et al. have updated this model utilizing modeling that was created for sputtered thin films[34]. It is important to remember that the strain which results from the RSC ($\epsilon^{RSC}_{(hkl)}$) and the strain that results from irradiation defects ($\epsilon^{total}_{(hkl)}$) make up the total strain. The two strain components are related by the following equation using the model that is extensively discussed in Refs.[32–34]:

$$\epsilon^{total}_{(hkl)} = \epsilon^{def}_{(hkl)}(1 + \alpha^{RSC}_{(hkl)}) \tag{3}$$

where $\alpha^{RSC}_{(hkl)}$ is a parameter that depends entirely on the material's elastic constants to characterize the RSC. Using the equations for anisotropic elasticity shown in Refs.[33,34], $\alpha^{RSC}_{(hkl)}$ for cubic crystals can be specified as:

$$\alpha^{RSC}_{(hkl)} = \frac{2C_{12} - C_{an}\Omega_{(hkl)}}{C_{11} + C_{an}\Omega_{(hkl)}} \tag{4}$$

where,

$$C_{an} = C_{44} - \frac{1}{2}(C_{11} - C_{12})$$
$$\Omega_{(hkl)} = 4(\alpha^2\beta^2 + \alpha^2\gamma^2 + \beta^2\gamma^2)$$
$$\alpha = \frac{h}{(h^2 + k^2 + l^2)^{1/2}}$$
$$\beta = \frac{k}{(h^2 + k^2 + l^2)^{1/2}}$$
$$\gamma = \frac{l}{(h^2 + k^2 + l^2)^{1/2}}$$

where $\Omega^{RSC}_{(hkl)}$ geometric component equal to 0 for the (1 0 0) planes[34] and C_{ij} are the stiffness constants. To find the true strain $\epsilon^{def}_{(hkl)}$ in the damaged zone and separate it from the "substrate strain" $\epsilon^{RSC}_{(hkl)}$ (a result of Poisson expansion), adjusted to hexagonal <0001> oriented system, we use the following relation[35]:

$$\alpha^{RSC} = \frac{C_{11} + C_{12} + C_{13}}{C_{11} + C_{12} - C_{13}} - 1 \quad (5)$$

From Eq. (3), it is possible to distinguish between the strain brought on by the RSC (resulting from purely elastic processes) and the strain imposed by the creation of irradiation defects. One of the main purposes of using the model is to separate the strain due to the defects and RSC, and to directly compare two different materials upon the same irradiation experiment. Using Eq. (4) for GaAs and Eq. (5) for 4H-SiC, the RSC factor (α^{RSC}) is calculated as ∼0.89 for GaAs and ∼0.19 for 4H-SiC, using stiffness constants given in Ref.[36]. It should be observed that the contribution of the RSC to GaAs is roughly 5 times more than its contribution to 4H-SiC.

Observations show that the maximum strain level in GaAs is much lower than that in 4H-SiC for the same introduced displacement damage by 300 keV Ar, quantified in terms of dpa. Further, based on the defect-strain and rigid substrate contribution model, an attempt is made to understand the response of irradiated surface layers of (upto ∼350 nm) 4H-SiC and GaAs crystals submitted to 300 keV Ar. Considering the difference in the RSC factors, it can be suggested that the strain due to the purely mechanical contribution after the creation of radiation-induced defects in GaAs is more than in 4H-SiC. For samples irradiated with 100 MeV Ag, Figs. 4(a) and 4(b) show how the total elastic strain maximum and defect-strain varies with the irradiation fluence. With increasing irradiation fluence, the strain for both materials increases until it falls for 4H-SiC and reaches saturation for GaAs.

V. CONCLUSION

The response of crystalline 4H-SiC and GaAs to ion irradiation has been studied using synchrotron HR-XRD in two separate energy regimes, and the elastic strain depth profiles have been evaluated using a dedicated XRD-pattern simulation computer code. First, the strain growth as a consequence of direct displacement damage after 300 keV Ar irradiation has been monitored. Results demonstrate that as soon as the amorphous regions build in 4H-SiC, the lattice strain saturates at a value of about 12% whereas, in GaAs, it reaches 0.88% but does not saturate within the experimental range of ion fluences. Additionally, for the same TRIM simulation-code estimated dpa values, the observed strain maximum in 4H-SiC is much higher than that observed in GaAs. It is demonstrated using proper modeling that the macroscopic mechanical behavior of GaAs exposed to ion irradiation contributes significantly to the local strain, whereas irradiation-produced defects can account for the majority of the local strain in 4H-SiC. Second, a comparison of the irradiation-induced strain in the high energy regime using 100 MeV Ag swift heavy ions has been carried out. The unique energy loss mechanism of 100 MeV Ag leaves several microns of the sub-surface region sparsely damaged. This makes it possible to study the role of elastic property on strain buildup due to the heavily damaged end of the ion range region, which is separated by several microns from the surface. After 100 MeV Ag irradiations in GaAs, the maximum strain increases from 0.17 to 0.37% with increasing fluence and then saturates. Whereas, the maximum lattice strain (4.6%) reduces for irradiation with fluences above 1×10^{13} Ag/cm^2 in 4H-SiC. . The coupling of displacement cascades and ionization-activated–thermally-assisted– The response of crystalline 4H-SiC and GaAs to ion irradiation has been studied using synchrotron HR-XRD in two separate energy regimes, and the elastic strain depth profiles have been evaluated using a dedicated XRD-pattern simulation computer code. First, the strain growth as a consequence of direct displacement damage after 300 keV Ar irradiation has been monitored. Results demonstrate that as soon as the amorphous regions build in 4H-SiC, the lattice strain saturates at a value of about 12% whereas, in GaAs, it reaches 0.88% but does not saturate within the experimental range of ion fluences. Additionally, for the same TRIM simulation-code estimated dpa values, the observed strain maximum in 4H-SiC is much higher than that observed in GaAs. It is demonstrated using proper modeling that the macroscopic mechanical behavior of GaAs exposed to ion irradiation contributes significantly to the local strain, whereas irradiation-produced defects can account for the majority of the local strain in 4H-SiC. Second, a comparison of the irradiation-induced strain in the high energy regime using 100 MeV Ag swift heavy ions has been carried out. The unique energy loss mechanism of 100 MeV Ag leaves several microns of the sub-surface region sparsely damaged. This makes it possible to study the role of elastic property on strain buildup due to the heavily damaged end of the ion range region, which is separated by several microns from the surface. After 100 MeV Ag irradiations in GaAs, the maximum strain increases from 0.17 to 0.37% with increasing fluence and then saturates. Whereas, the maximum lattice strain (4.6%) reduces for irradiation with fluences above 1×10^{13} Ag/cm^2 in 4H-SiC. . The coupling of displacement cascades and ionization-activated–thermally-assisted– The response of crystalline 4H-SiC and GaAs to ion irradiation has been studied using synchrotron HR-XRD in two separate energy regimes, and the elastic strain depth profiles have been evaluated using a dedicated XRD-pattern simulation computer code. First, the strain growth as a consequence of direct displacement damage after 300 keV Ar irradiation has been monitored. Results demonstrate that as soon as the amorphous regions build in 4H-SiC, the lattice strain saturates at a value of about 12% whereas, in GaAs, it reaches 0.88% but does not saturate within the experimental range of ion fluences. Additionally, for the same TRIM simulation-code estimated dpa values, the observed strain maximum in 4H-SiC is much higher than

that observed in GaAs. It is demonstrated using proper modeling that the macroscopic mechanical behavior of GaAs exposed to ion irradiation contributes significantly to the local strain, whereas irradiation-produced defects can account for the majority of the local strain in 4H-SiC. Second, a comparison of the irradiation-induced strain in the high energy regime using 100 MeV Ag swift heavy ions has been carried out. The unique energy loss mechanism of 100 MeV Ag leaves several microns of the subsurface region sparsely damaged. This makes it possible to study the role of elastic property on strain buildup due to the heavily damaged end of the ion range region, which is separated by several microns from the surface. After 100 MeV Ag irradiations in GaAs, the maximum strain increases from 0.17 to 0.37% with increasing fluence and then saturates. Whereas, the maximum lattice strain (4.6%) reduces for irradiation with fluences above 1×10^{13} Ag/cm^2 in 4H-SiC. When materials are exposed to swift heavy ions (SHIs), the strain in those materials cannot be sufficiently explained by considering only the elastic displacement damage. The coupling of displacement cascades and ionization leading to ionization-activated–thermally-assisted–defect-annealing (IATADA) has been proposed as the mechanism for the observed strain saturation/recovery behavior.

VI. SUPPLEMENTARY MATERIAL

The supplemental material contains figures showing the variation of TRIM dpa with depth for GaAs and 4H-SiC irradiated with 300 keV Ar. A figure supporting the claims about the strain in Ar irradiated 4H-SiC is also provided. Figures showing the depth dependence of the DW factors used in the RaDMaX program to simulate XRD curves are also included.

VII. ACKNOWLEDGEMENTS

The authors acknowledge the technical assistance of IUAC, New Delhi, India. The authors also thank the Department of Science and Technology, India for the financial support and the Jawaharlal Nehru Centre for Advanced Scientific Research, Bangalore, India, for facilitating the experiments at the Indian Beamline, Photon Factory, KEK, Japan.

DATA AVAILABILITY

The data that support the findings of this study are available from the corresponding author upon reasonable request.

REFERENCES

[1]W. Wesch and E. Wendler, *Ion Beam Modification of Solids*,(Springer, Berlin, 2016).
[2]E. Rimini, *Ion Implantation: Basics to Device Fabrication*, (Springer US, Boston, MA, 1995).
[3]A. Debelle, L. Thomé, I. Monnet, F. Garrido, O. H. Pakarinen and W. J. Weber, Phys. Rev. Materials **3**, 063609 (2019).
[4]A. Debelle, G. Gutierrez, A. Boulle, I. Monnet and L. Thomé, J. Appl. Phys. **132**, 085905 (2022).
[5]Y. Zhang, H. Xue, E. Zarkadoula, R. Sachan, C. Ostrouchov, P. Liu, X. lin Wang, S. Zhang, T. S. Wang, and W. J. Weber, Curr. Opin. Solid State Mater. Sci. **21**, 285 (2017).
[6]Y. Zhang and W. J. Weber , Appl. Phys. Rev. **7**, 041307 (2020).
[7]F. Roccaforte, P. Fiorenza, G. Greco, R. L. Nigro, F. Giannazzo, F. Iucolano and M. Saggio, M., Microelectronic Engineering **187**, 66-77 (2018).
[8]D. Lackner, T. Urban, R. Lang, C. Pellegrino, J. Ohlmann and V. Dudek,. Journal of Crystal Growth, **613**, 127201 (2023).
[9]`https://www.eeweb.com/600-v-new-generation-schottky-diodes/`
[10]`http://3-5pe.com/en/technology/`
[11]F. X. Zhang, Y. Tong, H. Xue, J. K. Keum, Y. Zhang, A. Boulle, A. Debelle and W. J. Weber, Appl. Phys. Lett. **114**, 221904 (2019).
[12]N. Sreelakshmi, P. Gupta, M. Gupta, V. R. Reddy, S. K. Rai, C. David and S. Amirthapandian, Materials Science in Semiconductor Processing **173**, 108170 (2024).
[13]S. Creutzburg, E. Schmidt, P. Kutza, R. Loetzsch, I. Uschmann, A. Undisz, M. Rettenmayr, F. Gala, G. Zollo, A. Boulle, A. Debelle, and E. Wendler, Phys. Rev. B **99**, 245205 (2019).
[14]A. Chakravorty, A. Boulle, A. Debelle, I. Monnet, G. Manna, P. Saha, M. K. Mukhopadhyay and D. Kabiraj, J. Mater. Sci. **57**, 20309 (2022).
[15]J.F. Ziegler, M.D. Ziegler and J.P. Biersack, Nucl. Instrum. Method Phys. Res., Sect. B **268**, 1818 (2010).
[16]W. J. Weber and Y. Zhang, Current Opinion in Solid State and Materials Science **23**, 100757 (2019).
[17]R. Devanathan, W. J. Weber, and F. Gao, J. Appl. Phys. **90**, 2303–2309 (2001).
[18]P. M. DeLuca, K. C. Ruthe and S. A. Barnett S A,Phys. Rev. Lett. **86**, 260–3 (2001).
[19]M. Souilah, A. Boulle and A. Debelle, J. Appl. Cryst. **49**, 311 (2016).
[20]A. Boulle and V. Mergnac, J. Appl. Cryst. **53**, 587 (2020).
[21]A. Chakravorty, H. Jatav, B. Singh, S. Ojha and D. Kabiraj, Materials Today: Proceedings **47**, 1633–1636 (2021).
[22]A. Chakravorty, Ch Dufour, A. Mishra, D. Kanjilal and D. Kabiraj, J. Phys. D: Appl. Phys. **55**, 505301 (2022).
[23]A. Chakravorty , B. Singh, H. Jatav, S. Ojha, J. Singh , D. Kanjilal and D. Kabiraj, J. Appl. Phys., **128** 165901 (2020).
[24]A. Chakravorty, Ch Dufour, B. Singh, H. Jatav, G. R. Umapathy, D. Kanjilal and D. Kabiraj, J. Appl. Phys. **130**, 165901 (2021).
[25]A. Chakravorty , B. Singh, H. Jatav, R. Meena, D. Kanjilal and D. Kabiraj, J. Appl. Phys. **129**, 245905 (2021).
[26]S. Qadri, M. Yousuf, C. Kendziora, B. Nachumi, R. Fischer, J. Grun, M. Rao, J. Tucker, S. Siddiqui, and M. Ridgway, Appl. Phys. A **79**, 1971–1977 (2004).
[27]S. Mishra, S. Bhaumik, J. Kumar Panda, S. Ojha, A. Dhar, D. Kabiraj and A. Roy, Nucl. Instrum. Method Phys. Res., Sect. B **316**, 192-197 (2013).
[28]Y. Zhang, H. Xue, E. Zarkadoula, R. Sachan, C. Ostrouchov, P. Liu, X. Wang, S. Zhang, T. S. Wang, and W. J. Weber, Curr. Opin. Solid State Mater. Sci. **21**, 285–298 (2017).
[29]H. Xue, Y. Zhang and W. J. Weber, Mater. Res. Lett. **5:7**, 494-500 (2017).
[30]M. Toulemonde, W. Assmann, Ch. Dufour, A Meftah, F. Studer and C. Trautmann, Mat. Fys. Medd. **52**, 263 (2006).
[31]G. Gaelle, M. Bricout, F. Garrido, A. Debelle, L. Roux and C. Onofri, J. Eur. Ceram. Soc. **42**, 6633-6641 (2022).

[32]A. Debelle and A. Declemy, Nucl. Instrum. Methods B **268**, 1460 (2010).
[33]S. I. Rao and C. R. Houska, J. Mater. Sci. **25**, 2822 (1990).
[34]A. Debelle, A. Boulle, F. Rakotovao, J. Moeyaert, C. Bachelet, F. Garrido and L. Thome, J. Phys. D: Appl. Phys. 46, 045309 (2013).
[35]I. Szlufarska, P. Voyles, K. Sridharan and Y. Katoh,. *Role of Defects in Swelling and Creep of Irradiated SiC* (No. DOE/NEUP–12-3357). Univ. of Wisconsin (2016).
[36]`Database:http://www.ioffe.ru/SVA/NSM/Semicond/`